Laser Diagnostic Investigation of the Bubble Eruption Patterns in the Freeboard of Fluidized Beds. 1. Optimization of Acetone Planar Laser Induced Fluorescence Measurements

Georg Hartung, Christoph R. Müller, Johan Hult, John S. Dennis, and Clemens F. Kaminski*

University of Cambridge, Department of Chemical Engineering, Pembroke Street, Cambridge CB2 3RA, United Kingdom

Here, the mixing of the freeboard gas with the gas of single bubbles and a continuous stream of bubbles is investigated using acetone planar laser induced fluorescence (PLIF), a technique only recently introduced to fluidized bed research [Solimene et al. *Chem. Eng. Sci.* **2007**, *62*, 94]. Various improvements with respect to laser diagnostics are presented leading to optimal signals from acetone PLIF. The results obtained are compared with models presented in the literature. The observed bubble eruption pattern generally corresponds to the models proposed by Levy and Lockwood [*AIChE J.* **1983**, *29*, 889], Yórquez-Ramirez and Duursma [*Powder Technol.* **2001**, *116*, 76], and Solimene et al. [*Chem. Eng. Sci.* **2007**, *62*, 94]. No difference was observed between the eruption patterns of a single bubble compared to a continuous stream of bubbles. In contrast to the models of Yórquez-Ramirez and Duursma and Solimene et al., five different patterns of the release of gas at a dome formed by a rising bubble are observed. An explanation for the formation of a thin layer of acetone after the eruption of a bubbles is given.

1. Introduction

Gas-fluidized beds are widely used in industry, e.g. in catalytic cracking, drying, and the gasification of coal and biomass. However, various aspects of the hydrodynamics of gas-fluidized beds are still relatively poorly understood. One of these is the eruption of bubbles at the surface of the bed and the subsequent mixing of the gas originating from the bubble with the gas in the freeboard. An understanding of the underlying physics of this process is not only important from an academic point of view but is also of enormous industrial relevance. This is particularly important where low-rank coal or biomass is being combusted. With these fuels, a significant proportion of their total content of carbon is released as bubbles of volatile matter.[1] Frequently, the material in these bubbles does not react completely within the bed, so that it is discharged into the freeboard when the bubble reaches the top surface. The volatile matter then reacts with oxygen from the air leaving the bed via homogeneous combustion in the freeboard. Consequently, the bubble induced mixing in the splash zone and freeboard becomes the rate limiting step.[8]

Despite the importance of the hydrodynamics of the freeboard, most studies have concentrated on the entrainment and elutriation of the bed particles.[5–7] However, there has been some work on the gas phase. For instance, two early models were proposed to describe the bubble eruption and subsequent disturbance of the freeboard: (i) the pulsed jet theory of Zenz and Weil[12] and (ii) the ghost bubble theory of Kehoe[17] and Pemberton and Davidson.[16] The pulsed jet theory[12] postulates that bubbles erupting at the surface behave as intermittent jets. This is depicted schematically in Figure 1a. These jets give rise to a highly irregular profile of gas velocity across the column. With height, the velocity fluctuations gradually dissipate and equilibrate to the superficial gas velocity.

The theory of ghost bubbles[16,17] is based on observations made of the eruption of bubbles at the top of a liquid fluidized bed and is depicted schematically in Figure 1b. Here, it is assumed that, after eruption, the bubble retains its shape, forming a "ghost bubble". The ghost bubble decelerates, as surrounding fluid is entrained in the rear of the bubble. Depending on whether the fluid is entrained in a laminar or turbulent manner, the ghost bubble becomes a vortex ring or a puff, respectively.[17] In Figure 1b, a puff is shown.

A separate bubble eruption model was proposed by Levy and Lockwood[11] based on the experimental observation of a toroidal circulation. This is shown in Figure 1c where, after the eruption of the bubble, the ejected bed particles reverse their flow direction and fall back into the bed. The drag force of these falling particles is then sufficient to cause a flow reversal in the surrounding gas. This downward motion creates a toroidal vortex, which moves initially toward the walls. This is followed by a vertical motion of the toroid, carried by the main flow in the freeboard. Solimene et al.[8,10] and Yórquez-Ramirez and Duursma[14] proposed very similar models to Levy and Lockwood,[11] but describing in more detail the release of the gas in the bubble upon the formation of a dome. Solimene et al.[8,10] reported the formation of a "nose pocket", the size of which depends on the size of the fluidized particles comprising the dome. The nose pocket is labeled "A" in Figure 1d. Beds of larger particles show larger nose pockets than beds of smaller particles. On the other hand, Yórquez-Ramirez and Duursma[14] proposed a rather evenly distributed release of gas along the surface of the dome of particles ocurring as a bubble erupts.

Experimentally, the pattern of bubble eruption can exhibit considerable variation. Hatano and Ishida[18] divided the patterns of bubbles bursting at the top of a fluidized bed into four categories: (i) isolated bubbles, (ii) successively rising bubbles, (iii) coalescing bubbles, and (iv) successively coalescing bubbles.

Progress in the understanding of bubble eruption and bubble induced turbulence in the freeboard has been hampered by the lack of appropriate experimental techniques. Early work on the measurement of the gas velocities in the freeboard made use of either hot wire anemometry[16] or laser Doppler anemometry.[9,11]

* To whom correspondence should be addressed. Tel.: +44 1223 334777. Fax +44 1223 334796. E-mail address: cfk23@cam.ac.uk.

10.1021/ie0713543 CCC: $40.75
Published on Web 07/03/2008

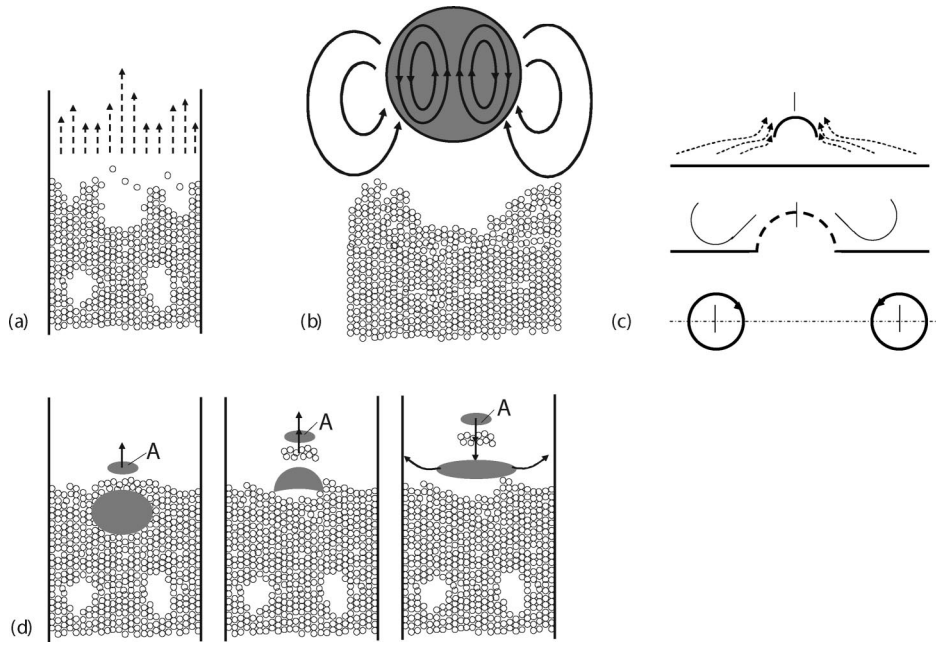

Figure 1. Schematic presentation of bubble eruption models reported in the literature. (a) "Pulsed-jet" model by Zenz and Weil.[12] (b) "Ghost-bubble" model of Pemberton and Davidson.[16] (c) Model of Levy and Lockwood.[11] (d) Model of Solimene et al.[8] The nose pocket is labelled "A".

However, these techniques are only able to provide point measurements. Measurement techniques, on the other hand, which provide instantaneous measurements of velocities and gas mixing in an entire plane, have been introduced to fluidized bed research.[8,10,14,15] These methods are usually based on two-dimensional laser sheet imaging techniques.

Laser diagnostic imaging techniques are nonintrusive and are capable of providing information about, for example, concentration, temperature and velocity fields. Planar laser induced fluorescence (PLIF) is therefore well suited for the study of freeboard hydrodynamics, as it permits highly sensitive concentration measurements of a tracer species seeded to a flow. The sensitivity of PLIF measurements makes it superior to other optical techniques for two reasons in this context: (1) The fluorescence signal is measured on a zero background in contrast to absorption techniques. Consequently, the sensitivity of fluorescence measurements is only limited by the shot noise and by the electronic noise of the detection device (e.g., noise of an intensifier noise). (2) The excitation wavelengths are commonly selected such that the detected fluorescence signal has a longer wavelength. Thus, Mie-scattering from contaminant particles or the ambient fluid can be eliminated simply by using a filter in front of the detection system, which will transmit the fluorescence wavelength but not the excitation wavelength.

In fluid mechanical applications, acetone-PLIF has been developed into a standard tool for mixture-fraction measurements.[21−32] The spectroscopic properties of acetone make it well-suited for use as a PLIF tracer molecule. Its broadband absorption (225−320 nm) is accessible with the fourth harmonic of high power Nd:YAG lasers, and the non-resonant visible fluorescence, emitted between 330 and 550 nm, can be collected with highly sensitive intensified charge-coupled device (ICCD) cameras. Acetone is characterized by a high vapor pressure at ambient temperature, thus allowing a high concentration seeding. Quantitative interpretation of the fluorescence signal is simplified by a fluorescence yield limited by rapid intersystem crossing, which reduces the importance of collisional quenching effects. Quantitative studies of mixing in flows which are isothermal and isobaric as in this work are straightforward, as a constant fluorescence yield can be assumed, which in turn means that the molar concentration is proportional to the intensity of the fluorescence signal. Despite the fact that acetone-PLIF has become a standard tool for applications in cold studies of jets and combustion processes, there are still several challenges for its application in fluidized beds to be achieved, amongst others, increasing the signal-to-noise ratios for acetone-PLIF measurements and performing the measurements as close as possible to the bed surface, where entrained fluidized particles complicate the signals.

The work reported here is an extension of the work of Solimene et al.[8] One objective was to introduce several optimization procedures yielding an excellent signal-to-noise (s/n)-ratio. A high acetone s/n-ratio becomes crucial if particle image velocimetry (PIV) is to be applied simultaneously with acetone PLIF, as the seeding particles of PIV cause a significant reduction in visibility through the glass windows, resulting in a decrease in acetone signal recorded by the ICCD camera. The simultaneous measurement of PIV and acetone-PLIF measurement are reported in a related paper.[33] Additional objectives are the study of the dynamics of bubble eruption of a continuous stream of bubbles and the report of bubble eruption profiles not reported by Solimene et al.[8] Also, a new explanation for the release of acetone after the eruption of a bubble is presented. This paper also serves as a basis for a follow-up study reporting on the simultaneous application of stereoscopic PIV and acetone PLIF measurements, which will provide information on both the flow field of the gas in the freeboard and the mixing of the gas initially contained in the erupting bubble.

2. Experimental Setup

2.1. Fluidized Bed and Particles. The fluidized bed was of square cross-section of side-length 200 mm and made of steel. A schematic diagram is given in Figure 2. The distributor consisted of an aluminum plate of 1.5 mm thickness, perforated with 81 holes, each of 0.5 mm diameter in a square array. The pressure drop over the distributor plate was larger than the weight of the bed per unit area, at minimum fluidization.

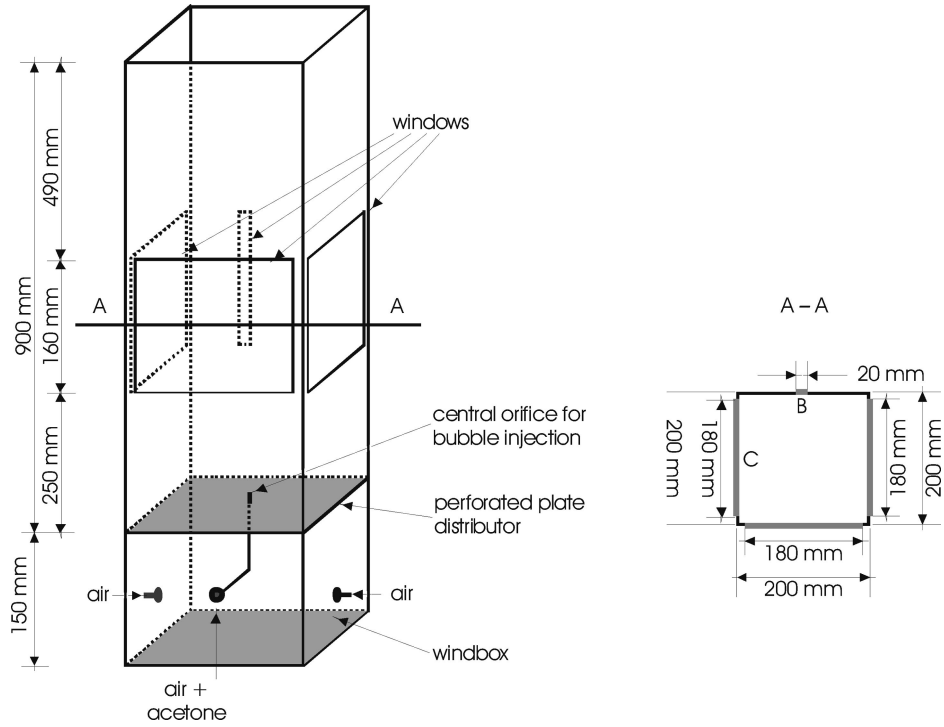

Figure 2. Schematic diagram of the fluidized bed used in this study.

The bed particles were glass ballotini sieved to size 150–250 μm; their measured U_{mf} was 28 mm/s when fluidized by laboratory air at 20 °C. The air was fed to the fluidized bed via a windbox, 150 mm in height. To inject single bubbles, or a stream of bubbles, into an incipiently fluidized bed, a nozzle of 10 mm i.d. and 13 mm o.d. was mounted in the center of the distributor plate as shown in Figure 2. To prevent particles from falling into the central orifice, it was covered by a brass mesh. To inject single bubbles, a controlled volume of gas was conveyed into the bed from a pressure vessel via a solenoid valve. The pressure in the vessel as well as the opening time of the valve could be varied. The overall height of the fluidized bed was 900 mm. The splash zone and freeboard were optically accessible. The laser sheet entered the system via a 20 × 160 mm glass window (labeled "B" in Figure 2) and resulting fluorescence was imaged though the 180 × 160 mm glass window, labeled "C" in Figure 2. The bed height at incipient fluidization was 250 mm, resulting in a bed aspect ratio of 1.25; a typical aspect ratio for, e.g., a fluidized bed gasifier.

2.2. Laser Diagnostic Arrangement. Planar laser-induced fluorescence (PLIF) of acetone (C_3H_6O) was studied in the freeboard of the fluidized bed. The diagnostic system consisted of a frequency quadrupled Nd:YAG laser (Continuum Surelite II) for the excitation of acetone at 266 nm and a high-resolution ICCD camera (Lavision Nanostar, 1280 × 1024 pixels, Germany), which was used to image the acetone-PLIF fluorescence signals. The images were digitized with 16-bit precision, with a true 12-bit dynamic range. The experimental setup is illustrated in Figure 3. The intensity of the fluorescence signal from the acetone is smaller than the Mie-scattering signal from the glass ballotini thrown into the freeboard upon bubble eruption, by several orders of magnitude. It is therefore crucial to suppress any residual laser radiation at wavelengths 1064 and 532 nm, which both pass through the frequency quadrupling unit of the laser. This was achieved using two Pellin−Broca prisms arranged in series. Pellin−Broca prisms offer the advantage of refracting light of different wavelengths at different angles, offering effective separation of the laser radiation of interest

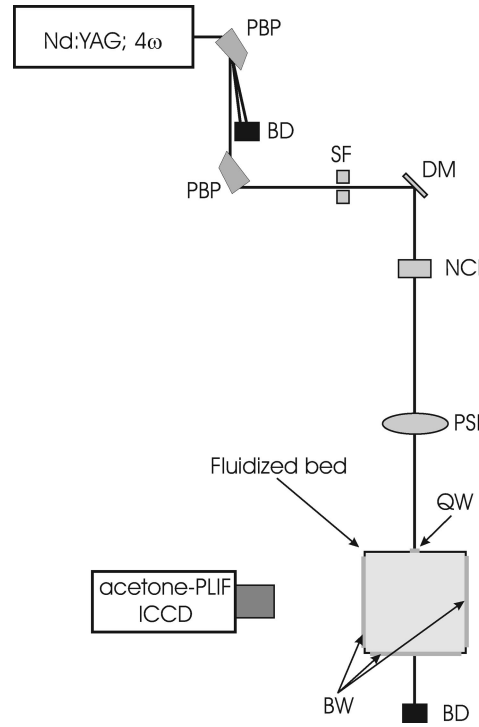

Figure 3. Schematic setup of the laser system employed for acetone-PLIF imaging. Description of optical components: PBP Pellin−Broca prism, BD beam dump, SF spatial filter, DM dichroic mirror, NCL negative cylindrical lens, PSL positive spherical lens, QW quartz window, BW B270 (Schott AG, Germany) window.

(266 nm) from the residual laser radiation at 1064 and 532 nm. The use of Pellin−Broca prisms leads to far superior rejection ratios of 532 and 1064 nm laser light compared to the use of dichroic mirrors, as commonly applied for this purpose.

The UV-laser beam (pulse energy: 60 mJ) was spatially filtered and expanded into a collimated sheet with a height of 60 mm and a thickness of 120 μm, using a cylindrical

planoconvex lens with focal length of $f = -25$ mm and a spherical lens with a focal length of $f = 500$ mm. A region 100 mm wide and 55 mm high was imaged using the ICCD; PLIF images were recorded at a repetition rate of 5 Hz. The camera was fitted with a *f*/1.2 camera lens (Nikkor) equipped with two WG 305 filters (Schott AG, Germany) and one BG 3 filter (Comar, UK). It is crucial to prevent any Mie-scattering signal at 266 nm from being recorded by the ICCD camera, as this could be erroneously interpreted as acetone PLIF signal. Therefore, two separate measures were taken to obviate this: (1) the use of two WG 305 filters rejects radiation at $\lambda = 266$ nm by a factor larger than 10^{10} and (2) the window, through which the acetone-fluorescence is imaged (B270, Schott AG, Germany), reduces the light at $\lambda = 266$ nm by another factor of 10^5. This arrangement also reduces the risk of overexposing the camera intensifier, which could cause irreversible damage. The BG 3 filter was employed to suppress radiation of wavelengths greater than 470 nm from reaching the detection device.

Both, the Nd:YAG laser and the ICCD camera, were triggered from a programmable timing unit, which was controlled by software (Davis 6.2, Lavision, Germany). The Davis software in turn was triggered from a 40 MHz arbitrary waveform generator (TGA1242, TTi, UK). The recorded acetone-PLIF images were first corrected for background and laser sheet inhomogeneities. Subsequently, noise was reduced by applying a median filter.

3. Acetone PLIF Optimization

Initial experiments yielded insufficient s/n-ratios in the acetone-PLIF images. However, several modifications were made, as described below, which resulted in s/n-ratios of about 80, which was regarded as sufficiently high for the analysis of the phenomena in the freeboard:

(1) A 2 × 2 hardware-binning of the CCD chip resulted in a gain in s/n-ratio of about 4. One binned pixel represented an area of 155 μm × 155 μm in the measurement plane. The remaining pixel matrix of 640 × 512 pixels was observed to yield good s/n-ratio with a sufficient resolution in order to analyze the apparent flow motions. In previous studies Solimene at al.[8] used a pixel resolution of 400 μm × 400 μm.

(2) A commercial acetone-nozzle seeder, as commonly applied in combustion research and used for initial investigations, was replaced by an acetone bubbler. The acetone bubbler consisted of a vessel of 40 L filled with 15 L of 10 mm diameter glass spheres. This vessel was then filled with acetone so that the spheres were just fully covered with acetone. The glass spheres prevent large bubbles being formed in the acetone and entraining liquid droplets into the fluidized bed. This could possibly result in distorted acetone concentrations in the PLIF-results. The temperature of the vessel was controlled at 47 °C by means of a water bath to ensure a sufficient concentration of acetone in the injected bubbles. The line from the bubbler to the nozzle was heated to prevent condensation.

(3) In order to reduce the loss of acetone from the injected bubbles by mass transfer to the particulate phase gas, the expanded height of the bed was kept below 250 mm. If significant transfer occurs, there is loss of contrast between the resulting ghost bubble and the gas leaving the top of the particulate phase. Solimene et al.[8] used a bed height of 350 mm.

(4) The thickness of the laser sheet was adjusted by careful selection of lenses to about 120 μm. Since the binning of the CCD-chip, mentioned above, resulted in a pixel resolution of 155 × 155 μm, the thickness of the laser sheet was thus less than the in-plane resolution. It is important to note that the effective in-plane pixel resolution cannot be larger than the thickness of the laser sheet.

(5) The size of the particles fluidized was carefully selected. Mie-scattering approximately scales with the second power of the radius of the particles. A similar dependence is found for the minimum fluidization velocity, U_{mf}. By using larger particles, higher gas flow rates can be employed, and thus, a higher turnover rate of the freeboard volume is possible. Consequently, large acetone concentration gradients in the freeboard are obtained, which is desirable. However, the intensity of the parasitic 266 nm Mie-scattering signal may be increased to such levels that the camera intensifier will be damaged irreversibly — and vice versa. Thus, a compromise has to be found by performing careful test runs with the particular diagnostic setup employed to find its limits. In initial experiments, it was found that the risk of damaging the camera could be reduced to an acceptable level using the type of glass ballotini and range of flow rates described in the previous section.

(6) To obtain a high precision in the calibration of the PLIF signal with acetone concentration, a collimated laser sheet was used. Collimated laser sheets require a lens diameter equivalent to the laser sheet dimension.

4. Experimental Results

Bubbles of diameters $D_e = 30-50$ mm were injected into the gas-fluidized bed. The rise velocity of a single bubble, U_b, in an incipiently fluidized bed is given by $U_b = 0.71\sqrt{(gD_e)}$. Thus, the ratio U_{mf}/U_b was ∼1/14−1/18, indicating that the bubbles were "fast" and consequently that the cloud of the released bubbles was very thin.[34] Also Solimene et al.[8] reported thin clouded bubbles in their experiments. From our measurements, it was observed that the size of the dome formed by a stream of bubbles was of comparable size to the ones formed when single bubbles were injected into a fluidized bed. Thus, bubbles in the continuous stream were of similar diameter to those obtained when single bubbles were injected. The individual bubbles in a train of bubbles are therefore also expected to have thin clouds. Due to the thin cloud only very little exchange between the gas in the bubble and the gas in the emulsion phase is expected. Furthermore, diffusion of the acetone from the bubble during its rise though the bed (∼0.5 s) is expected to be negligible.[8]

In the following, for each acetone-PLIF image in a figure, the 97.5% maximum concentration $C_{max,\,97.5}$, was determined from a probability density function of the acetone-concentration distribution. $C_{max,\,97.5}$ is defined as the acetone concentration which is larger than 97.5% of the acetone concentration in an individual acetone-PLIF image. All acetone-images within a figure were normalized to the maximum of these values. The colorscale employed for all figures presenting acetone-PLIF images is illustrated in Figure 4.

4.1. Single Bubble Injected into a Bed of Geldart Group B Particles. Figures 4 and 5 show PLIF measurements of the eruption of one single bubble, injected into the bed at incipient fluidization. The first part of the bubble eruption event is shown in Figure 4, and the second part is shown in Figure 5. The coordinate y is vertically upward, and x is measured horizontally. The origin of the coordinate systems is the center of the bed at the surface of the fluidized bed. To avoid any damage to the ICCD camera from Mie scattering, the field of view of the camera started at 6 mm above the surface of the bed. Figures 4 and 5 were acquired using a "side setup" of the

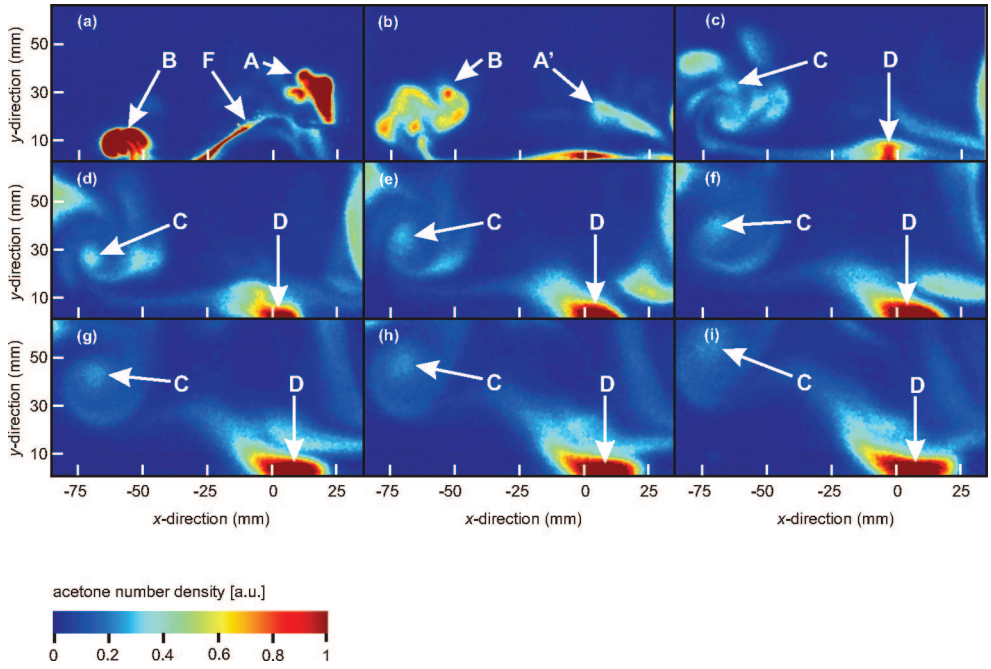

Figure 4. PLIF images of a single bubble, $D_e = 45$ mm, erupting at the top of an incipiently fluidized bed. The time between two successive images is 0.2 s, which is the repetition rate of the PLIF measurements.

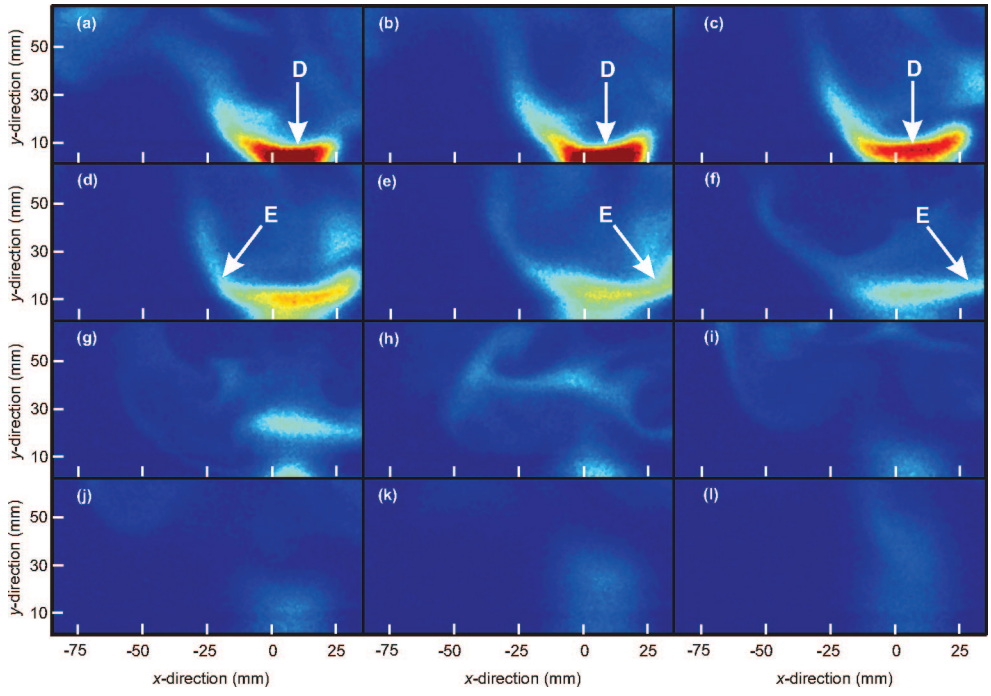

Figure 5. Continuation of the PLIF images of the bubble eruption shown in Figure 4. The time between two successive images is now 0.4 s, i.e. only every second acquired frame is shown.

camera, i.e. the camera as shifted toward one side of the bed, so that the field of view extended to one wall. A "central setup" of the cameras has been also applied and it was found that the eruption profiles were symmetric.[33] Thus, imaging mainly one side of the eruption events did not cause any loss of information. However, the side setup can be beneficial, as the entire flow field at one side of the axis of symmetry is imaged. The diameter of the bubble was $D_e \sim 45$ mm. From Figures 4 and 5, the following stages in the eruption of a bubble injected into an incipiently fluidized bed can be observed:

• The bubble, forms a dome (labeled "F") as it reaches the top surface of the fluidized bed, as seen in Figure 4a.

• A pocket of gas is released at roughly the center of the dome, as can be seen in Figure 4a. Solimene et al.[8] refer to this pocket as the nose pocket. The nose pocket is labeled "A".

• In Figure 4a and b, acetone is also visible at the outer margins of the dome, labeled "B". Another structure similar to the one labeled B would be seen to the right of the dome but is outside the field of view. During this time, the position of the nose pocket does not vary significantly. Some acetone from the nose pocket diffuses to the surroundings, leading to a reduction of acetone signal. However, it is quite clear that the nose pocket does not move upward; in fact it moves slightly downward, as seen in Figure 4b, labeled "A". This is caused by the high

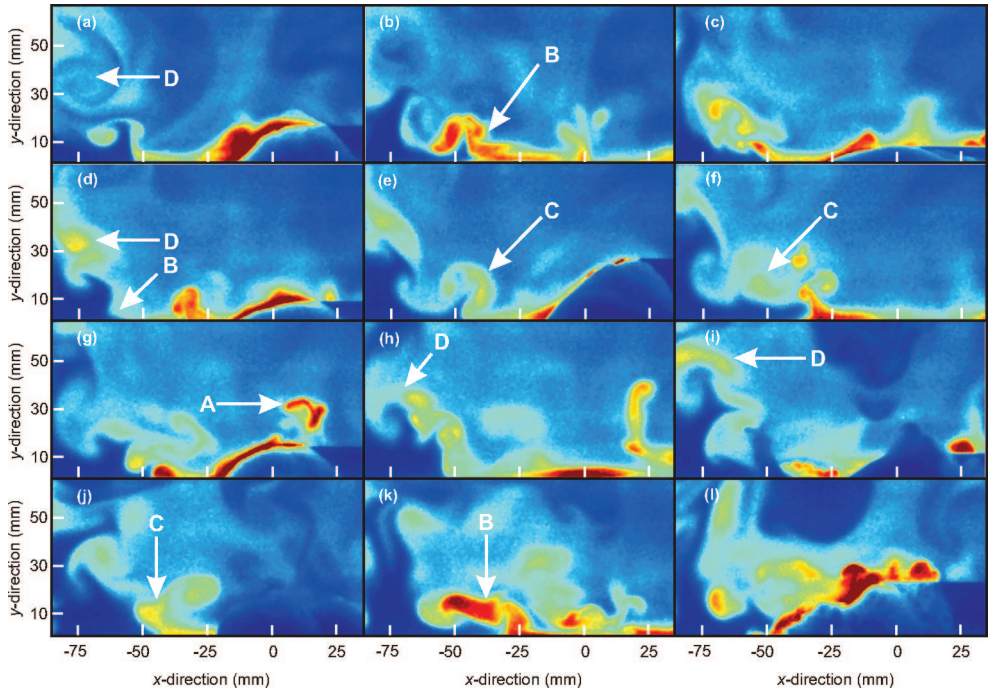

Figure 6. PLIF images of a continuous stream of bubbles released into an incipiently fluidized bed recorded at 5 Hz. The flow rate through the central nozzle was 50 cc/s, i.e. the orifice velocity, $U_O = 0.63$ m/s.

velocity of the surrounding gas moving downward toward the volume previously occupied by the dome. This behavior is presented in detail elsewhere.[33]

• The gas, originally present in the bubble, released at the margins of the collapsed dome, moves toward the walls, exhibiting a complex structure as it does so. The strong horizontal motion close to the surface of the fluidized bed is shown in Figure 4a−c (horizontal motion of the structure labeled "B"). The two vortex rings, i.e. the cross-section of a toroidal vortex, rotate in opposite directions, i.e clockwise at the left wall and counterclockwise at the right wall. One of these can be seen in Figure 4c labeled "C". Due to the rotation and rise of the vortices, acetone is subsequently shed from the initially confined region of acetone (Figure 4c−i), leading to a more even distribution of acetone along the bed (shedding and dispersion of the structure labeled C). The two vortices are then carried upward by the main flow field in the freeboard.

• Just as the vortices initially formed at the wall rise upward and shed small pockets of gas, a new region of acetone forms at the surface of the bed right at the position where the bubble originally erupted, as seen in Figure 4d and labeled "D". Shortly after the appearance of this new source of acetone, some acetone moves convectively and, or, diffusively in the vertical direction. However, quite surprisingly, the vertical motion of the acetone is quite limited. From Figure 4g onward, the gas released at the top of the bed is shed at the outer margins of "D". The width and the height of D was ∼30 and ∼10 mm, respectively. The structure denoted by D is surprisingly stable, persisting from Figure 4a through to Figure 5d. The actual center of the freeboard contains only a little acetone and most of the acetone seems to be released along a concave curve upward and toward the walls.

• It is only after a significant amount of time has elapsed, i.e. ∼3.2 s, after the eruption of the bubble, that the layer of acetone formed at D detaches from the top surface of the fluidized bed as seen in "E" in Figure 5d and is carried into the freeboard, where it finally mixes with the surrounding fluid, leading to a dispersion of the acetone signal. However, some acetone escaping from the bed can survive for up to ∼5.5 s after the eruption of the bubble, as seen in Figures 5e−l.

4.2. Injection of a Continuous Stream of Bubbles into an Incipiently Fluidized Bed. Figure 6 shows PLIF measurements of the eruption of a stream of bubbles continuously formed at the central orifice. The bed was held at minimum fluidization and the flow rate through the 10 mm central orifice was 50 cc/s, i.e. the orifice velocity, $U_O = 0.63$ m/s. On the basis of the size of the dome, the bubble diameters are estimated to be in the range of ≈35−50 mm. Again, the ICCD camera was shifted toward one side of the bed, so that the field of view included one wall. From Figure 6, the following phenomena can be observed:

• Similar to the results from the injection of single bubbles, most of the gas from the bubble is released at the outer margins, labeled "B", of the dome initially formed.

• Upon collapse of the dome, Figure 6a and b, a toroidal vortex forms. The two vortices seen as a cross-section of the toroidal vortex are carried horizontally just above the surface of the fluidized bed toward the walls. The left-hand vortex is labeled "C" in Figure 6; the right-hand one is outside the field of view.

• Sometimes the occurrence of a small nose pocket can be observed, e.g. in Figure 6g labeled "A", but it is much less pronounced than is the case with single bubbles.

• In the vicinity of the walls, the vortices are carried upward owing to the main flow in the freeboard. During this upward motion, each vortex entrains surrounding gas and little gas pockets are shed, leading to a decreased turbulent energy and acetone signal, as seen at "D" in Figure 6h.

• The strongest acetone signal is usually observed at the position where the dome forms and roughly along a concave curve upward and toward the walls. Close to the walls, directly above the surface of the fluidized bed, very little acetone can be found. Here, only acetone-free gas is released into the freeboard.

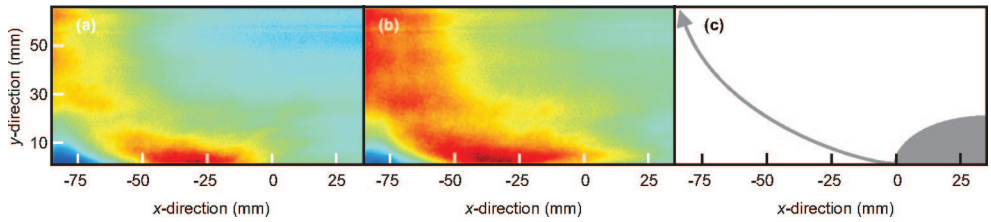

Figure 7. Time-averaged PLIF images of the eruption of a continuous stream of bubbles for two different flow rates through the central nozzle: (a) 50 cc/s, i.e. $U_O = 0.63$ m/s and (b) 67 cc/s, i.e. $U_O = 0.86$ m/s. A schematic diagram of the time-averaged acetone profile is shown in part c. The grey shaded shape in the form of a quarter disk represents the position of the occurrence of most of the domes.

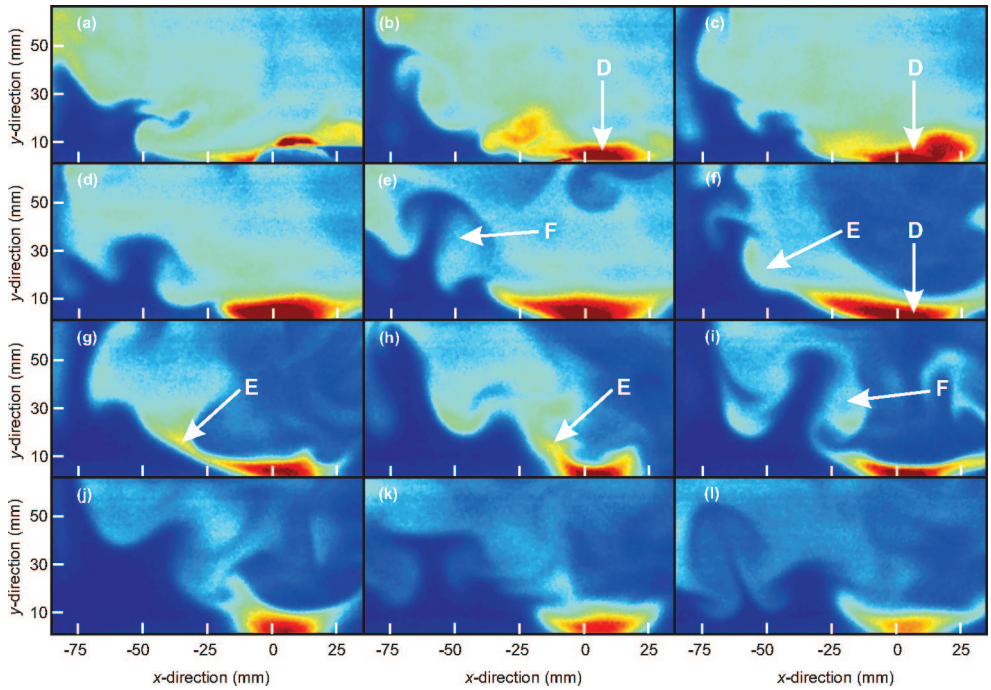

Figure 8. PLIF images taken after a continuous stream of bubbles has been shut off. The time delay between successive images is 0.4 s. The last bubble erupting before the shut off of continuous stream of bubbles is shown in part a.

• Observations of a large number of image sequence, such as these in Figure 6, showed that gas, upon formation of the dome, is released in three principal ways: (i) formation of a nose pocket at the surface of the dome, (ii) release of gas along the entire surface of the dome, and (iii) release predominantly at the margin of the dome without the formation of a nose pocket.

Time-averaged images of the acetone signal are shown in Figure 7. In Figure 7a and b, the bed was kept at minimum fluidization and the flow rate through the central 10 mm orifice was 50 and 67 cc/s, respectively, corresponding to orifice velocities of $U_O = 0.63$ m/s and $U_O = 0.86$ m/s, respectively. The images shown in Figure 7a and b were produced by time-averaging over ~70 s. It is quite clear that, on a time averaged basis, most of the acetone can be found directly at the surface of the fluidized bed in the center and along a concave curve upward and toward the walls, as depicted schematically in Figure 7c. The gray shaded shape in the form of a quarter disk, indicates the occurrence of most of the domes. The layer at the top of the fluidized bed where a high concentration of acetone can be found is, however, fairly thin, only ~10 mm in Figure 7. Comparing Figure 7a with b, it can be seen that the thickness increases with increasing flow rate. Quite surprisingly, there is very little acetone in the center of the fluidized bed for $0 < x < 25$ mm and $y = 0$ mm, i.e. the place where the dome forms. This is consistent with observations made in Figure 6, as most of the gas is released at the outer margins the dome (regardless of the release of gas upon formation of the dome), then first carried horizontally toward the walls, before rising upward close to the walls. The fact that the domes are not symmetrical about $x = 0$ mm can be explained by examining Figure 6. It can be observed that bubbles tend to erupt toward positive values along the x-direction. In the vicinity of the walls, at the surface of the fluidized bed, only very little acetone can be found. This is expected as gas percolating close to the walls through the fluidized bed, kept at incipient fluidization, will be too distant from the central jet to participate in any exchange of the gas phase in the bubble and the bed.

4.3. Cessation of a Continuous Stream of Bubbles. The behavior of the acetone concentration in the freeboard of a fluidized bed after the acetone-laden bubble stream has been stopped is interesting, as shown in Figure 8. The first image in Figure 8 shows the last bubble of the stopped stream of bubbles erupting. This shows that, after the continuous stream of bubbles is stopped, no further formation of domes can be observed, since the fluidized bed is kept at incipient fluidization. The last bubble eruption is shown in Figure 8a. However, the formation of a layer of acetone at the center of the top of the fluidized bed can be observed in Figure 8b−l, labeled "D". Initially, the width and thickness of this band is ~50 and ~10 mm, respectively (Figure 8d). With time, acetone is shed, labeled "E". This continuous shedding leads to a subsequent reduction in the width and thickness of the acetone layer. At the end of the time series

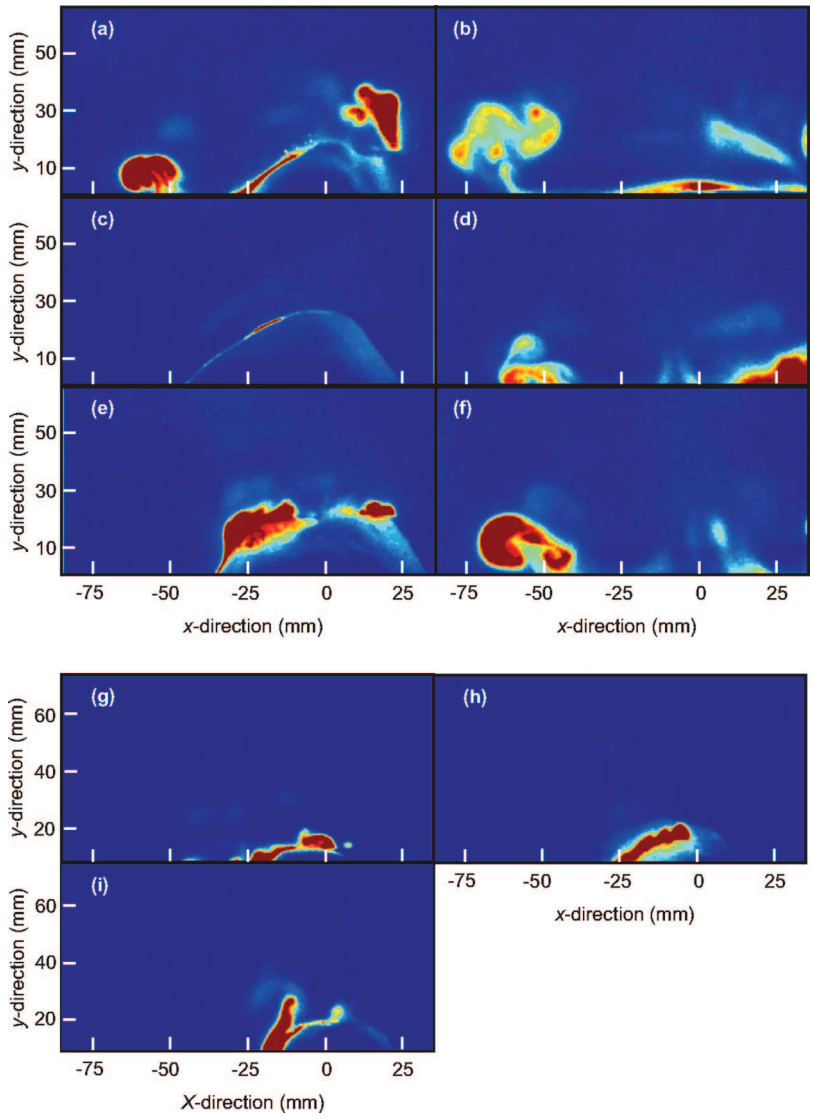

Figure 9. PLIF images of eruption profiles observed for single bubble injection experiments. The profiles were divided into the following patterns: (i) formation of a nose pocket, one bubble eruption event is shown in parts a and b; (ii) no escape of gas observable along the dome, one bubble eruption event is shown in parts c and d; (iii) acetone mainly escapes at an eruption angle of ~45°; one bubble eruption event is shown in parts e and f; (iv) the release of gas is evenly distributed along the dome (parts g and h); and (v) gas is mainly released at an eruption angle of ~90°, shown in part i.

shown in Figure 8, the width and thickness of the acetone layer is only ~20 and ~5 mm, respectively. Only very little acetone is released into the center of the freeboard. In fact, it can be observed in Figure 6f that the center of the fluidized bed becomes completely free of acetone-laden air. All of these observations are in good agreement with observations of the eruption of a single bubble. Due to the high s/n ratio, another very interesting phenomenon can be seen in Figure 8, namely the formation of Rayleigh−Taylor type instabilities. For example, in Figure 8d and e, labeled "F", the formation of a mushroomlike area of acetone can be observed, which propagates into the acetone-rich part of the freeboard. The formation of Rayleigh−Taylor instabilities is expected as the acetone-rich air, which lies above the acetone-free air, is denser than the latter.

It should be noted that the formation of a small pocket of gas at the center of the dome of the erupting bubble is not the only "eruption profile" that was observed. In Figures 9 and 10, several alternative eruption profiles, are shown, respectively, for single bubble injection and continuous bubble stream experiments. These eruptions can be divided into five different groups; schematic diagrams of the different eruption profiles are shown in Figure 11 and described below:

(i) Formation of one or more nose pockets at the center of the dome formed by the erupting bubble. It was, however, observed that the size of the nose pocket can vary significantly. For example, a small pocket is shown in Figure 10a, whereas a comparatively large nose pocket can be seen in Figure 9a. This is schematically depicted in Figure 11a.

(ii) Gas is released evenly along the dome, i.e., no preferred location of acetone release is observed (Figures 9g and h, 10g and h, and 11c).

(iii) Gas mainly escapes from some location along the side of the dome. The location of release can vary, but is quite often to be found at an angle of eruption of ~45° (Figures 9e, 10e and f, and 11e).

(iv) Gas mainly escapes at the outer margin of the dome, i.e. at an angle of eruption of 90°, as seen in Figures 9i, 10i, and 11d. It should be emphasized that this only describes the release of gas during the formation of the dome (and sometimes very early stages of dome collapse). Regardless of the bubble eruption

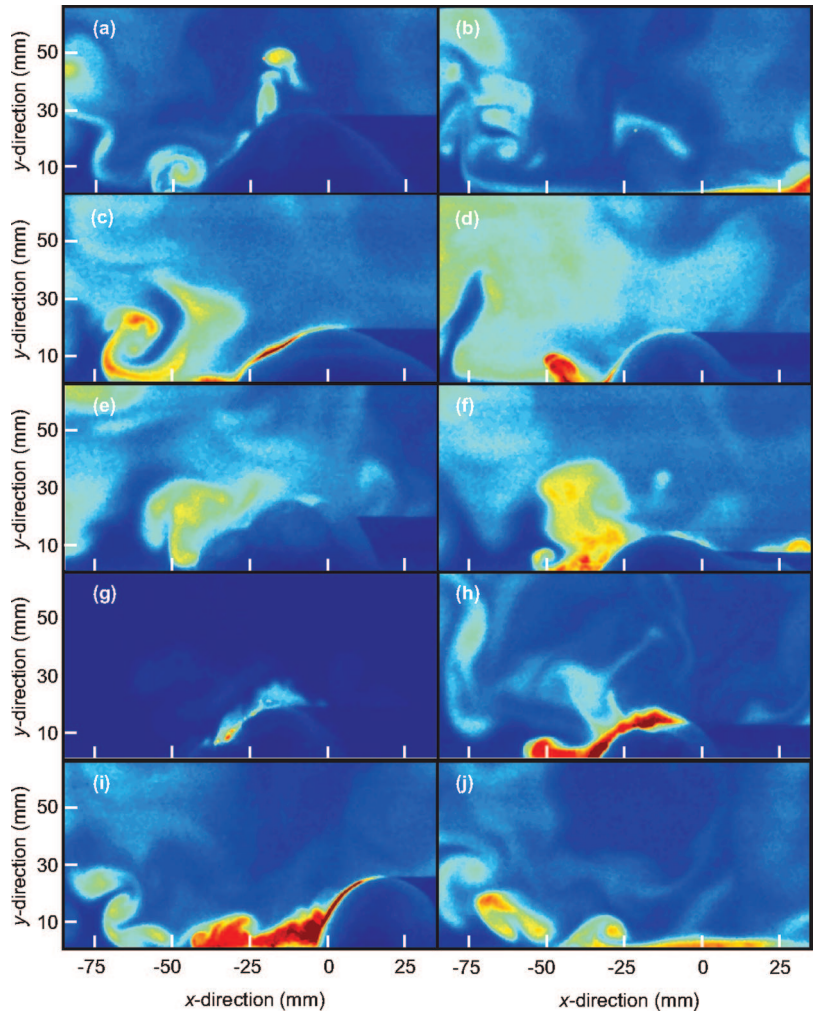

Figure 10. PLIF images of eruption profiles observed for a continuous stream of bubbles. The flow rate through the central nozzle was 50 cc/s, i.e. the orifice velocity was $U_O = 0.63$ m/s. The profiles were divided into the following patterns: (i) formation of a nose pocket (one bubble eruption event shown) parts a and b; (ii) no escape of gas observable along the dome, parts c and d; (iii) acetone mainly escapes at an eruption angle of ~45°, (two bubble eruption events are shown) parts e and f; (iv) the release of acetone is evenly distributed along the dome (one bubble eruption event is shown), parts g and h; and (v) acetone is mainly released at an eruption angle of ~90° (one bubble event is shown), parts i and j.

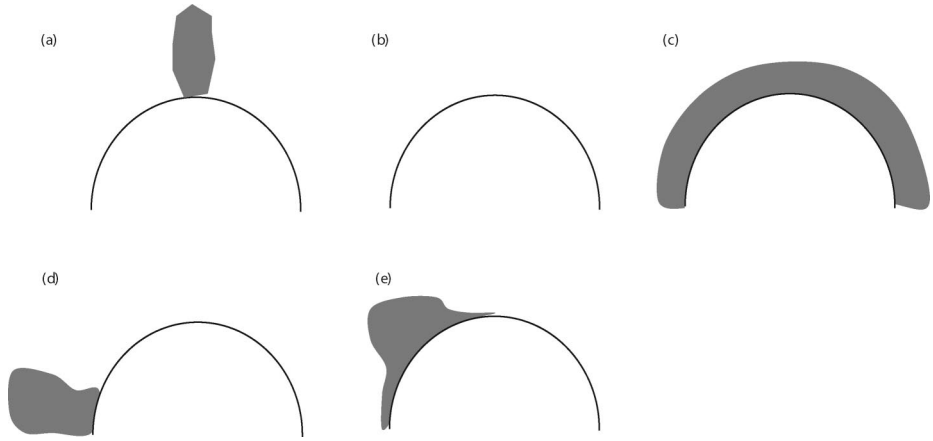

Figure 11. Schematic diagram of the eruption pattern observed in this study. The grey indicates the release of gas upon formation of the dome: (a) formation of a nose pocket, (b) no release of gas, (c) even release of gas along the dome, (d) the majority of the gas is released at an eruption angle of ~90°, (e) the majority of the gas is released at an eruption angle of ~45°.

profile, the majority of the gas is always released at the outer margin of the dome, upon the collapse of the dome.

(v) Almost no gas escapes from the dome. One might argue that this has occurred while the dome was still developing, i.e., that the bubble was not close to eruption. However, this eruption pattern was also observed at fairly well developed dome heights, so it is believed that this can be considered as a separate eruption pattern. Furthermore, after the collapse of the dome no acetone was observed at the center of the bed for such an eruption pattern. This is shown in Figures 9c and d, 10c and d, and 11b.

It is quite interesting that all five eruption patterns were observed in experiments where (i) a single bubble was injected

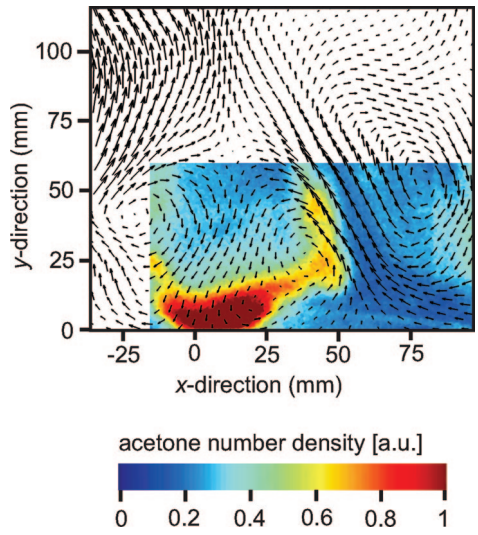

Figure 12. Simultaneous PIV and acetone-PLIF measurements. The vectors indicate the flow, whereas the colour represents the acetone signal intensity.

and (ii) where a stream of bubbles was released in an incipiently fluidized bed. Thus, the eruption pattern seems to be independent of the mechanism of bubble release.

For completeness, Figure 12 shows simultaneous PIV and acetone-PLIF measurements. In Figure 12 the shedding of two vortices from the layer of acetone which form after the eruption of a single bubble. However, a detailed presentation and discussion of the simultaneously acquired PIV and acetone-PLIF measurement is given in ref 33.

5. Discussion

In this study, the eruption of (i) single bubbles and (ii) a continuous stream of bubbles was investigated using acetone-PLIF measurements. The optimization of the acetone fluorescence signal level is crucial to enable the simultaneous acquisition of acetone PLIF and stereoscopic PIV, which is reported elsewhere.[33] This will provide not only information about the gas mixing but also about the instantaneous flow field.

The observations made from Figures 4 and 5 in this study show that most of the gas from the erupting bubble is released at the outer margin of the dome, i.e. at an eruption angle of ~90°. As the dome collapses, the falling particles cause the gas, due to momentum exchange between the particles and the surrounding gas, also to move downward. This downward motion of the surrounding gas forces the gas of the erupting bubble to escape mainly toward the sides of the collapsing dome, leading to a strong horizontal motion of the gas originally present in the erupting bubble. This motion leads to the formation of a toroidal vortex. The left and right part of the vortex (seen as a cross-section) rotate, respectively, clockwise and anticlockwise, resulting in a negative vertical gas velocity at the center of the fluidized bed. Near the walls, the vortices are carried upward by the main flow of the gas leaving the top of the fluidized bed. As they rise through the freeboard, the vortices mix with the surrounding fluid and shed little pockets of gas, consequently losing their turbulent energy as they do so. Owing to this eruption profile, only very little acetone is observed at the center of the fluidized bed at heights >20 mm above the bed's surface. Averaging over several bubble eruption events, as in Figure 7, showed that the flow profile in the freeboard, introduced by the bubble eruption events, causes the majority of the acetone being present along a concave curve upward and toward the walls, as depicted schematically in Figure 7c. These general trends in the bubble eruption pattern are in agreement with the observation of Levy and Lockwood,[11] Yorquez-Ramirez and Duursma,[14] and Solimene et al.[8] Neither ghost bubbles nor a flow profile consistent with the pulsed-jet model of Zenz and Weil[12] were observed. Comparing Figures 4–6, there does not seem to be a phenomenological difference between the eruption of a single bubble and a stream of bubbles.

After the collapse of the dome of a single injected bubble, a layer of acetone appears on the surface of the fluidized bed. From this layer, acetone is continuously shed into the freeboard, resulting in a decrease in the width of the layer. The acetone layer is present for a comparatively long time of ~3.2 s, as seen in Figure 5d and e. This layer eventually detaches from the surface of the bed and is carried into the freeboard by the main flow, where it disperses into the surrounding gas. However, from Figure 5f−l, it can be seen that the release of some of this acetone can be delayed for as long as ~5.5 s after the eruption of the bubble. Of course, this acetone layer cannot be observed during the eruption of a continuous stream of bubbles. However, Figure 8 shows that after a continuous stream of bubbles is stopped, exactly the same phenomena can be observed. Solimene et al.[8] suggested that molecular diffusion is probably responsible for this, as the thickness of the cloud of the bubble is very small. Here, another mechanism is proposed. As the ratio of rise velocity of the bubbles to superficial fluidizing velocity exceeds 10, the clouds of the injected bubbles and the bubbles in the continuous bubble stream are very thin.[34] So, very little gas exchange between the gas phase in the bubble and the emulsion phase would be expected. However, this is probably only true if the bubble is spherical, but not if the wake angle is <180°, which would be expected from experimental results.[13,35] Theoretical potential flow calculations of the gas circulation pattern around an indented bubble,[36] i.e. bubbles with a wake, indicate that, depending on the size of the wake angle, even for thin clouded bubbles, gas exchange between the gas phase in the bubble and the emulsion would be expected. Experimental evidence for this theory has been reported by Rowe,[37] using an air bubble containing NO_2. Besides the formation of a cloud, a colored column reaching from the distributor up to the wake of the bubble can be observed. The thickness of the column is ~1/3−1/4 of the maximum diameter of the bubble. The bubble under investigation[37] was injected into a 2D bed and had a wake angle of ~120°. Thus, it would be expected that during the rise of the bubble through the fluidized bed, there is exchange between the gas in the bubble and the emulsion phase, resulting in acetone being mixed into the emulsion phase. However, acetone in the emulsion phase will percolate through the bed with a significantly smaller velocity than the bubble rise velocity, namely U_{mf}/ε_{mf}. With a bed height of H_{mf} = 250 mm, the risetime, t_r, of the acetone mixed with the emulsion phase is $t_r = H_{mf}\varepsilon_{mf}/U_{mf}$ = 3.6 s, which is in good agreement with the release time reported here of 3.2 s.

In contrast to Solimene et al.'s[8] observations, different patterns of gas release upon formation of the dome were observed. For a similar particle size as used in this study, Solimene et al.[8] only reported the formation of a nose pocket, which they attributed to through flow of gas from the bubble into the freeboard during the formation of the dome. In our study, various release patterns of gas were observed and could be classified into five different patterns, with the release of a nose pocket being just one of them. We agree with the explanation of Solimene et al.[8] for the formation of a nose

pocket; however, the through-flow of gas upon formation of the dome should not be restricted to just the nose of the dome. It has been reported that, in 2D beds, the thickness of the dome is not uniform along the angle of eruption.[13] It has been observed that the dome often breaks, i.e. the dome thickness is less than three particle diameters thick, close to the nose of the dome.[13] The formation of a nose pocket would be expected if the dome breaks at its nose. However, it was reported[13] that the dome can also break at eruption angles $\neq 0°$, which would lead to different eruption patterns, e.g. the release of gas at an eruption angle of $\sim 45°$. In fact, it can be expected that in the case of a 3D bed, the local dome thickness is more complex than in the case of a 2D bed. It is assumed that the eruption pattern of gas upon the formation of the dome, observed in this study, depends on the local thickness of the dome.

6. Conclusions

An acetone-PLIF technique has successfully been employed to visualize bubble eruption events at the top of a fluidized bed. Several optimization measures were taken to optimize the s/n ratio in order to achieve a s/n ratio high enough to allow such measurements to be performed simultaneously with PIV in the future, as the seeding particles will reduce the visibility through the windows, resulting in a significant decrease in signal.

The eruption of single bubbles and a stream of bubbles released into an incipiently fluidized bed was investigated. The eruption pattern of a single bubble did not differ from that of a stream of bubbles. Our observations are in agreement with the eruption model of Levy and Lockwood,[11] Yórquez-Ramarez and Duursma,[15] and Solimene et al.[8] The only difference between our observations and the model proposed by Yórquez-Ramarez and Duursma[15] and Solimene et al. [8] is in the release of gas at the dome of an erupting bubble. Solimene et al.[8] only reported the release of a nose pocket, whereas Yórquez-Ramarez and Duursma[15] assumed an even release of gas. However, in this study five different release patterns of gas have been identified. The different release patterns were attributed to variations in the local thickness of the dome formed as a bubble breaks through the surface of the bed. This thickness can vary significantly from one bubble to the next. Our experimental observations contradict the ghost bubble theory[16,17] and the pulsed-jet theory.[12] This is in agreement with the experimental findings of others.[8,11,15]

A new explanation is proposed for the observation that a layer of acetone persists at the surface after the eruption of a bubble. It is proposed that the layer of acetone at the surface of the fluidized bed forms due to gas exchange between the gas in the bubble and the emulsion phase. This can be explained as the wake angle of the bubbles is $<180°$. On the basis of theoretical potential flow calculations of Collins[36] and experimental observations in 2D beds of Rowe,[37] the formation of a column of acetone reaching from the distributor up to the wake of the bubbles is expected. Acetone from this column will be carried up the bed with a significantly smaller velocity than the rise velocity of a bubble, namely U_{mf}/ε_{mf}. This continuous transport of acetone is then observed as a thin layer at the surface of the fluidized bed. It is assumed that formation of such a column is increased with decreasing wake angle.

Acknowledgment

This work was supported by grants from the EPSRC and grants from EUs Sixth Framework Programme Intellect D.M. contract (EU Project AST3-CT-2003-502961, Jan 01, 2004−Dec 31, 2007). G.H. is grateful to a case studentship from CMI (Cambridge−MIT Institute) and Intellect D.M. C.R.M. acknowledges financial support from the Deutscher Akademischer Austauschdienst (DAAD) and Cambridge European Trust. J.H. was supported by an Advanced Research Fellowship from the EPSRC (EP/C012399/1). C.F.K. is thankful to the Leverhulme Trust for personal sponsorship.

Literature Cited

(1) Scott, S. A.; Davidson, J. F.; Dennis, J. S.; Hayhurst, A. N. The devolatilisation of particles of a complex fuel (dried sewage sludge) in a fluidise bed. *Chem. Eng. Sci.* **2007**, *62*, 584–598.

(2) Reference deleted during production.

(3) Reference deleted during production.

(4) Reference deleted during production.

(5) Li, J. L.; Kato, K. A correlation of the elutriation rate constant for adhesive particles (group C particles). *Powder Technol.* **2001**, *118*, 209–218.

(6) Santana, D.; Rodriguez, J.; Macias-Machin, A. Modelling fluidized bed elutraition of fine particles. *Powder Technol.* **1999**, *106*, 110–118.

(7) Choi, J. H.; Suh, J. M.; Chang, I. Y.; Shun, D. W.; Son, J. E.; Kim, S. D. The effect of fine particles on elutriation of coarse particles in a gas fluidized bed. *Powder Technol.* **2001**, *26*, 190–194.

(8) Solimene, R.; Marzocchella, A.; Ragucci, R.; Salatino, P. Laser diagnostics of hydrodynamics and gas-mixing induced by bubble bursting at the surface of gas-fluidized beds. *Chem. Eng. Sci.* **2007**, *62*, 94–108.

(9) Hamdullahpur, F.; MacKay, G. D. M. Two-phase flow behaviour in the freeboard of a gas-fuidized bed. *AIChE J.* **1986**, *32*, 2047–2055.

(10) Solimene, R.; Marzocchella, A.; Ragucci, R.; Salatino, P. Flow structure and gas-mixing induced by bubble bursting at the surface of an incipiently gas-fluidized bed. *Ind. Eng. Chem. Res.* **2004**, *43*, 5738–5753.

(11) Levy, Y.; Lockwood, F. C. Laser doppler measurements of flow in freeboard of a fluidized bed. *AIChE J.* **1983**, *29*, 889–895.

(12) Zenz, F. A.; Weil, N. A. A theoretical-empirical approach to the mechanism of particle entrainment from fluidized beds. *AIChE J.* **1958**, *4*, 472–479.

(13) Müller, C. R.; Davidson, J. F.; Dennis, J. S.; Hayhurst, A. N. A study of the motion and eruption of a bubble at the surface of a two-dimensional fluidized bed using particle image velocimetry (PIV). *Ind. Eng. Chem. Res.* **2007**, *46*, 1642–1652.

(14) Yorquez-Ramirez, M. I.; Duursma, G. R. Insights into the instantaneous freeboard flow above a bubbling fluidised bed. *Powder Technol.* **2001**, *116*, 76–84.

(15) Duursma, G. R.; Glass, D. H.; Rix, S. J. L.; Yorquez-Ramirez, M. I. PIV investigations of flow structures in the fluidised bed freeboard region. *Powder Technol.* **2001**, *120*, 2–11.

(16) Pemberton, S. T.; Davidson, J. F. Elutriation from fluidized beds - 1. Particle ejection from the dense phase into the freeboard. *Chem. Eng. Sci.* **1986**, *41*, 243–251.

(17) Kehoe, P. W. K. The effect of particle size on slugging fluidised beds. PhD disseration, University of Cambridge, UK, 1969.

(18) Hatano, H.; Ishida, M. The entrainment of solid particle from a gas-solid fluidized bed. *J. Chem. Eng. Jpn.* **1981**, *14*, 306.

(19) Reference deleted during production.

(20) Reference deleted during production.

(21) Su, L. K.; Clemens, N. T. Planar measurements of the full three-dimensional scalar dissipation rate in gas-phase turbulent flows. *Exp. Fluids* **1999**, *27*, 507–521.

(22) Lozano, A. Laser-excited luminescent tracers for oplanar concentration measurements in gaseous jets. Ph.D. thesis, Stanford University, Department of Mechanical Engineering, Stanford, CA, 1992.

(23) Thurber, M. C.; Hanson, R. K. Pressure and composition dependences of acetone laser-induced fluorescence with excitation at 248, 266, and 308 nm. *Appl. Phys. B* **1999**, *69*, 229–240.

(24) Hult, J.; Richter, M.; Nygren, J.; Aldén, M.; Hultqvist, A.; Christensen, M.; Johansson, B. Application of a high-repetition-rate laser diagnostic system for single-cycle-resolved imaging in internal combustion engines. *Appl. Opt.* **2002**, *41* (24), 5002–5014.

(25) Hultqvist, M. Christensen, B. Johansson, M. Richter, J. Nygren, J. Hult, and Aldén, M. *The HCCI Combustion Process in a Single Cycle -- High-Speed Fuel Tracer LIF and Chemiluminescence Imaging*; SAE Paper No. 2002-01-0424, The Society of Automotive Engineers: Warrendale, PA, 2002.

(26) Patrie, B. J.; Seizman, J. M.; Hanson, R. K. Instantaneous three-dimensional flow visualization by rapid acquisition of multiple planar flow images. *Opt. Eng.* **1994**, *33*, 975–980.

(27) Moreau, J.; Boree, J.; Bazile, R.; Charnay, G. Destabilisation of a compressed vortex by a round jet. *Exp. Fluids* **2004**, *37* (6), 856–871.

(28) Thurber, M. C.; Hanson, R. K. Simultaneous imaging of temperature and mole fraction using acetone planar laser-induced fluorescence. *Exp. Fluids* **2001**, *30* (1), 93–101.

(29) Meyer, T. R.; King, G. F.; Martin, G. C.; Lucht, R. P.; Schauer, F. R.; Dutton, J. C. Accuracy and resolution issues in NO/acetone PLIF measurements of gas-phase molecular mixing. *Exp. Fluids* **2002**, *32* (6), 603–611.

(30) Koch, J. D.; Hanson, R. K. Temperature and excitation wavelength dependencies of 3-pentanone absorption and fluorescence for PLIF applications. *Appl. Phys. B* **2003**, *76* (3), 319–324.

(31) Grossmann, F.; Monkhouse, P. B.; Riddler, M.; Thurber, M. C.; Grisch, F.; Kirby, B. J.; Votsmeier, M.; Hanson, R. K. Measurements and modeling of acetone laser-induced fluorescence with implications for temperature-imaging diagnostics. *Appl. Opt.* **1998**, *37* (21), 4963–4978.

(32) Yip, B.; Miller, M. F.; Lozano, A.; Hanson, R. K. A combined OH/acetone planar laser--induced fluorescence imaging technique for visualizing combusting flows. *Exp. Fluids* **1994**, *17*, 330–336.

(33) Müller, C. R.; Hartung, G.; Davidson, J. F.; Hult, J.; Kaminski, C. F.; Dennis, J. S. Laser diagnostic investigation of the bubble eruption patterns in the freeboard of fluidized beds. Part 2: Simultaneous acetone PLIF and stereoscopic PIV measurements. Submitted to *AIChE J.*

(34) Davidson, J. F.; Harrison, D. *Fluidised particles*; Cambridge University Press: New York, 1963.

(35) Müller, C. R.; Holland, D. J.; Davidson, J. F.; Dennis, J. S.; Gladden, L. F.; Hayhurst, A. N.; Mantle, M. D.; Sederman, A. J. Rapid two-dimensional imaging of bubbles and slugs in a three-dimensional, gas-solid, two-phase flow system using ultrafast magnetic resonance. *Phys. Rev. E* **2007**, *75*, 020302 (R)

(36) Collins, R. An extension of Davidson's theory of bubbles in fluidized beds. *Chem. Eng. Sci.* **1965**, *20*, 747–755.

(37) Rowe, P. N. Private communication. Atomic Energy Research Establishment, Harwell. The image is shown in ref 34.

Received for review October 8, 2007
Revised manuscript received March 6, 2008
Accepted March 12, 2008

IE0713543